

Non-Gaussianity in WMAP Data Due to the Correlation of CMB Lensing Potential with Secondary Anisotropies

Erminia Calabrese^{1,2}, Joseph Smidt², Alexandre Amblard², Asantha Cooray²,
Alessandro Melchiorri¹, Paolo Serra², Alan Heavens³, Dipak Munshi^{3,4}

¹*Center for Cosmology, Dept. of Physics & Astronomy,
University of California Irvine, Irvine, CA 92697.*

²*Physics Department and INFN, Universita' di Roma "La Sapienza", Ple Aldo Moro 2, 00185, Rome, Italy*

³*Scottish Universities Physics Alliance (SUPA), Institute for Astronomy,
University of Edinburgh, Blackford Hill, Edinburgh EH9 3HJ, UK and*

⁴*School of Physics and Astronomy, Cardiff University, CF24 3AA*

We measure the skewness power spectrum of the Cosmic Microwave Background (CMB) anisotropies optimized for a detection of the secondary bispectrum generated by the correlation of the CMB lensing potential with integrated Sachs-Wolfe effect and the Sunyaev-Zel'dovich effect. The covariance of our measurements is generated by Monte-Carlo simulations of Gaussian CMB fields with noise properties consistent with Wilkinson Microwave Anisotropy Probe (WMAP) 5-year data. When interpreting multi-frequency measurements we also take into account the confusion resulting from unresolved radio point sources. We analyze Q, V and W-band WMAP 5-year raw and foreground-cleaned maps using the KQ75 mask out to $l_{\max} = 600$. We find no significant evidence for a non-zero non-Gaussian signal from the lensing-secondary correlation in all three bands and we constrain the overall amplitude of the cross power spectrum between CMB lensing potential and the sum of SZ and ISW fluctuations to be 0.42 ± 0.86 and 1.19 ± 0.86 in combined V and W-band raw and foreground-cleaned maps provided by the WMAP team, respectively. The point source amplitude at the bispectrum level measured with this skewness power spectrum is higher than previous measurements of point source non-Gaussianity. We also consider an analysis where we also account for the primordial non-Gaussianity in addition to lensing-secondary bispectrum and point sources. The focus of this paper is on secondary anisotropies. Consequently the estimator is not optimised for primordial non-Gaussianity and the limit we find on local non-Gaussianity from the foreground-cleaned V+W maps is $f_{\text{NL}} = -13 \pm 62$, when marginalized over point sources and lensing-ISW/SZ contributions to the total bispectrum.

PACS numbers: 98.80.-k 95.85.Sz, 98.70.Vc, 98.80.Cq

I. INTRODUCTION

The all-sky, multi-frequency WMAP maps of Cosmic Microwave Background (CMB) anisotropies [1] have presented cosmologists with an opportunity to test the cosmological scenario of structure formation at an unprecedented accuracy. The results on the CMB temperature and polarization angular power spectra are in very good agreement with the expectations of the standard cosmological model of structure formation based on primordial, adiabatic and scale invariant perturbations, and cold dark matter [2].

In addition to measuring the angular power spectrum and cosmological parameter estimates from it [3], WMAP CMB maps are now routinely used to constrain statistical properties of the CMB beyond the simple two-point angular correlation function. These studies include tests of cosmological isotropy [4, 5, 6], topology [7, 8], and non-Gaussianity [9, 10, 11, 12], among other tests. In the standard cosmological model, primordial CMB anisotropies are supposed to be Gaussian, however non-Gaussianities may be present in the observed CMB maps through a combination of primordial non-Gaussianity of density perturbations generated during inflation [13, 14, 15, 16, 17], the imprint of non-

linear growth of structures as probed by secondary effects [18, 19], and mode-coupling effects by secondary sources of temperature fluctuations such as gravitational lensing of the CMB [20, 21].

The detection of these non-Gaussian features will not only provide additional useful information on the parameters of the standard cosmological model but also allow independent tests on constraining the amplitude of primordial non-Gaussianity due to non-standard initial conditions and, ultimately, inflation after accounting for secondary non-Gaussian signals generated since last scattering. Several recent studies have made use of the bispectrum for the study of non-Gaussianities [9, 12]. This quantity involves a three-point correlation function in Fourier or multipole space. The configuration dependence of the bispectrum $B(k_1, k_2, k_3)$ with lengths (k_1, k_2, k_3) that form a triangle in Fourier space can be used to separate various mechanisms for non-Gaussianities, depending on the effectiveness of the estimator used.

In most CMB non-Gaussianity studies [1, 12, 22] the estimator employed involves a measurement that compresses all information of the bispectrum to a single number called the cross-skewness computed with two weighted maps. Such a drastic compression limits the ability to study the angular dependence of the non-Gaussian signal and to separate any confusing fore-

grounds from the primordial non-Gaussianity. More recently, some of us have introduced a new estimator that preserves some angular dependence of the bispectrum [23, 24]. This recently led to a new measurement of the primordial non-Gaussianity parameter [9].

The skewness power spectrum is indeed a weighted statistic that can be tuned to study a particular form of non-Gaussianity, such as what may arise either in the early Universe during inflation or late-times during structure formation, while retaining information on the nature of non-Gaussianity more than the skewness alone. When applied to the CMB data, this allows a way to explore all non-Gaussian signals, including those generated by contaminants such as Galactic foregrounds and unresolved point sources.

In this paper we analyze the recent WMAP data for the skewness power spectrum associated with cross-correlation between lensing and ISW and SZ effects, respectively. The presence of a measurable signal in this secondary non-Gaussianity, especially with the cross-correlation of lensing with the SZ effect, was identified in 2003 by Goldberg & Spergel [20, 21]. We provide first constraints on this signal from WMAP data using Q, V and W-band maps both in the ‘‘Raw’’ and foreground ‘‘Clean’’ form as provided by the WMAP team publicly.

After accounting for the confusion from point sources generated by the overlap of the point source shot-noise bispectrum and the lensing-secondary anisotropy cross-correlation bispectrum, we find no significant detection of the lensing effect in existing WMAP data. We constrain the overall normalization of the lensing-SZ and lensing-ISW angular cross-power spectra to be 0.42 ± 0.86 and 1.19 ± 0.86 in combined V and W-band raw and foreground-cleaned maps provided by the WMAP team, respectively. The point source amplitude we determine from the raw map of Q-band with $b_{\text{src}} = (67.8 \pm 5.4) \times 10^{-25} \text{ sr}^2$ is higher than the estimate by the WMAP team with $(6.0 \pm 1.3) \times 10^{-5} \mu\text{K}^3\text{-sr}^2$ [2] (the value we determine is $(13.7 \pm 1.1) \times 10^{-5} \mu\text{K}^3\text{-sr}^2$ in the same units used by the WMAP team). We find similarly a factor of 2 increase in the results from the V-band map. In the case of clean maps, we find $b_{\text{src}} = (6.2 \pm 5.4) \times 10^{-25} \text{ sr}^2$, which is smaller than the WMAP team’s estimate with clean maps for the Q band with $(4.3 \pm 1.3) \times 10^{-5} \mu\text{K}^3\text{-sr}^2$ [2] (the value we determine is $(1.4 \pm 1.1) \times 10^{-5} \mu\text{K}^3\text{-sr}^2$ in the same units used by the WMAP team). We find similar differences in the V and W bands as well. It is unclear exactly where these differences come from. We do not employ the same E-statistic that is optimized for point sources as the WMAP team in the present study.

We also considered the extent to which primordial non-Gaussianity confuse the detection of lensing-secondary correlations and found that when including f_{NL} in model fits, in addition to point sources, leads to a factor of 2 degradation in the error of the amplitude of lensing-secondary correlation power spectrum.

This paper is organized as follows: in the next Section, we review the measurement theory. We refer the reader

to Munshi et al. [25] for more details. In Section III we present our results and discuss the evidence for the secondary non-Gaussianity in WMAP data.

II. SKEWNESS POWER SPECTRUM ESTIMATOR

If we consider three statistically isotropic fluctuation fields, say temperature anisotropies but weighted with different window functions differently, $X(\hat{\Omega})$, $Y(\hat{\Omega})$ and $Z(\hat{\Omega})$ described by the multipole moments $a_{l_1 m_1}^X, a_{l_2 m_2}^Y, a_{l_3 m_3}^Z$, all the information available in the three-point correlation function is contained in the angular bispectrum $B_{l_1 l_2 l_3}^{XYZ}$ defined by a triangle in multipole space with lengths of sides (l_1, l_2, l_3) :

$$B_{l_1 l_2 l_3}^{XYZ} = \sum_{m_1, m_2, m_3} \begin{pmatrix} l_1 & l_2 & l_3 \\ m_1 & m_2 & m_3 \end{pmatrix} \langle a_{l_1 m_1}^X a_{l_2 m_2}^Y a_{l_3 m_3}^Z \rangle . \quad (1)$$

Since measuring the full bispectrum is challenging, many previous measurements have focused mostly on the skewness which is collapse of information in the bispectrum in some way to a single number. As discussed in Munshi et al. [25], it is useful to pursue instead the skewness power spectrum which can be considered as the angular power spectrum of the correlation of the product map $X(\hat{\Omega})Y(\hat{\Omega})$ and the $Z(\hat{\Omega})$. In the absence of sky-cut and instrumental noise, we can write the skewness power spectrum as :

$$\langle a_{lm}^{XY} a_{l'm'}^Z \rangle \equiv C_l^{XY,Z} \delta_{ll'} \delta_{mm'} , \quad (2)$$

where a_{lm}^{XY} is the spherical harmonic transform coefficient of the field XY .

It is possible to show that this quantity, in the homogeneity and isotropy assumption, is directly connected with the mixed bispectrum associated with these three fields according to the relation [23] :

$$C_l^{XY,Z} = \sum_{l_1, l_2} B_{ll_1 l_2}^{XYZ} w_{l_1 l_2} \sqrt{\frac{(2l_1 + 1)(2l_2 + 1)}{4\pi(2l + 1)}} \begin{pmatrix} l_1 & l_2 & l_3 \\ 0 & 0 & 0 \end{pmatrix} \quad (3)$$

where $w_{l_1 l_2}$ is a filter function that needs to be introduced in a more general approach and represents the spherical transform of the mask. This power spectrum contains information about all possible triangular configuration when one of the side is fixed at length l .

We can now relate the X , Y and Z fields introduced above to quantities that we are interested in studying. We therefore expand the observed CMB temperature anisotropies $\delta T(\hat{\Omega})$ in terms of the primary anisotropy δT_P , due to lensing of primary δT_L , and the other secondaries generated by the low-redshift large-scale structure δT_S :

$$\delta T(\hat{\Omega}) = \delta T_P(\hat{\Omega}) + \delta T_L(\hat{\Omega}) + \delta T_S(\hat{\Omega}) . \quad (4)$$

Expanding these fields in the Fourier space according to :

$$\begin{aligned}\delta T_P(\hat{\Omega}) &= \sum_{lm} a_{Plm} Y_{lm}(\hat{\Omega}), \\ \delta T_L(\hat{\Omega}) &= \sum_{lm} \nabla \Theta(\hat{\Omega}) \cdot \nabla T_S(\hat{\Omega}), \\ \delta T_S(\hat{\Omega}) &= \sum_{lm} a_{Slm} Y_{lm}(\hat{\Omega})\end{aligned}\quad (5)$$

we have an expression for the cross-correlation power-spectra which denotes the coupling of lensing with a specific form of secondary CMB anisotropies. Their bispectrum is given by :

$$\begin{aligned}B_{l_1 l_2 l_3}^{PLS} &= \sum_{m_1 m_2 m_3} \begin{pmatrix} l_1 & l_2 & l_3 \\ m_1 & m_2 & m_3 \end{pmatrix} \times \\ &\times \langle (\delta T_P)_{l_1 m_1} (\delta T_L)_{l_2 m_2} (\delta T_S)_{l_3 m_3} \rangle\end{aligned}\quad (6)$$

where $(\delta T)_{lm}$ is the anisotropy map expansion to multipole harmonics [20, 21, 26]. With explicit calculations, the bispectrum becomes :

$$\begin{aligned}B_{l_1 l_2 l_3}^{PLS} &= - \left\{ X_{l_3} C_{l_1} \frac{l_2(l_2+1) - l_1(l_1+1) - l_3(l_3+1)}{2} + \right. \\ &\left. + perm. \right\} \sqrt{\frac{(2l_1+1)(2l_2+1)(2l_3+1)}{4\pi}} \begin{pmatrix} l_1 & l_2 & l_3 \\ 0 & 0 & 0 \end{pmatrix}\end{aligned}\quad (7)$$

where X_{l_3} is the lensing potential and secondary anisotropies cross-correlation power spectrum and C_{l_1} is the unlensed power spectrum of CMB anisotropies.

A. Optimised skew spectrum

Following the discussion in Munshi et al. [25], we define a set of 9 different fields of weighed temperature :

$$A_{lm}^1 = \frac{b_l a_{lm}}{\tilde{C}_l b_l^2 + N_l} C_l ; \quad B_{lm}^1 = \frac{l(l+1) b_l a_{lm}}{\tilde{C}_l b_l^2 + N_l} ; \quad C_{lm}^1 = X_l \frac{b_l a_{lm}}{\tilde{C}_l b_l^2 + N_l}\quad (8a)$$

$$A_{lm}^2 = -\frac{l(l+1) b_l a_{lm}}{\tilde{C}_l b_l^2 + N_l} C_l ; \quad B_{lm}^2 = \frac{b_l a_{lm}}{\tilde{C}_l b_l^2 + N_l} ; \quad C_{lm}^2 = X_l \frac{b_l a_{lm}}{\tilde{C}_l b_l^2 + N_l}\quad (8b)$$

$$A_{lm}^3 = \frac{b_l a_{lm}}{\tilde{C}_l b_l^2 + N_l} C_l ; \quad B_{lm}^3 = \frac{b_l a_{lm}}{\tilde{C}_l b_l^2 + N_l} ; \quad C_{lm}^3 = -X_l \frac{l(l+1) b_l a_{lm}}{\tilde{C}_l b_l^2 + N_l},\quad (8c)$$

where b_l is the beam transfer function; N_l is the noise power spectrum as obtained from averaging noise maps simulations; C_l and \tilde{C}_l are the unlensed and the lensed CMB power spectrum, respectively.

From these harmonic coefficients, we also construct 9 sky maps :

$$\begin{aligned}A^i(\hat{\Omega}) &= \sum_{lm} Y_{lm}(\hat{\Omega}) A_{lm}^i, \\ B^i(\hat{\Omega}) &= \sum_{lm} Y_{lm}(\hat{\Omega}) B_{lm}^i, \\ C^i(\hat{\Omega}) &= \sum_{lm} Y_{lm}(\hat{\Omega}) C_{lm}^i\end{aligned}\quad (9)$$

where $i = 1, 2, 3$.

The skewness power spectrum that is weighted to measure non-Gaussianity associated with lensing-secondary correlation can be written as :

$$C_l^{2,1} = \frac{1}{2l+1} \sum_m \sum_i \text{Real} \left[\left(A^i(\hat{\Omega}) B^i(\hat{\Omega}) \right)_{lm} C^i(\hat{\Omega})_{lm} \right]\quad (10)$$

The above form is exact for all-sky measurements. To account for partial sky coverage due to the Galactic and foreground mask and inhomogeneous noise, we also cal-

culate the linear-order correction terms from Ref. [25] :

$$\begin{aligned}C_l^{2,1} &= \frac{1}{f_{sky}} \sum_i \left[C_l^{AB,C} - C_l^{A<B,C>} - C_l^{B,<A,C>} + \right. \\ &\left. - C_l^{<AB>,C} \right]^i.\end{aligned}\quad (11)$$

The term above without an averaging is the direct estimate from data while the averaged corrective terms such as $C_l^{A<B,C>}$ are obtained by cross-correlating the product of the observed A map with the simulated B and C maps and then taking an ensemble average over many realizations. The reduction in the sky are due to mask is corrected dividing by the observed sky fraction f_{sky} .

As discussed in Ref. [25], it is possible to show that this quantity is directly related to the bispectrum :

$$C_l^{2,1} = \frac{1}{2l+1} \sum_{l_1 l_2} \frac{\hat{B}_{ll_1 l_2} (B_{ll_1 l_2}^{PLS})^c}{\tilde{C}_l \tilde{C}_{l_1} \tilde{C}_{l_2}},\quad (12)$$

where $\hat{B}_{ll_1 l_2}$ is the total bispectrum in the data and $(B_{ll_1 l_2}^{PLS})^c$ is the shape of the bispectrum that we have employed by weighting the A, B and C maps. This bispectrum is equal to the form written in equation (7), with

permutations only restricted to $l_1 \rightarrow l_2$ while l_3 is kept fixed to X_{l_3} .

We assume the total bispectrum present in the data is a combination of the both the lensing-secondary bispectrum and contaminations such as point sources. When fitting to measurements, we will construct the map C^i in above by appropriately weighting it with X_l to study the cross-correlation of lensing potential with SZ and ISW separately. We assume that the bispectrum in the data is composed by these two effects with two unknown amplitudes relative to the prediction under the fiducial cosmological model. The comparison between the data and the modeled expectation will be used to determine the two relative

III. DATA ANALYSIS

We summarize our analysis in the following steps:

A. Data and Simulations

We have considered the WMAP 5-year Stokes-I raw and clean sky maps for the Q, W and V frequency bands, obtained from the public lambda website¹. We use the Healpix's synfast code [27] to generate 250 CMB temperature anisotropy Gaussian maps giving in input the WMAP 5-year best-fit CMB anisotropy power spectrum with cosmological parameters: $H_0 = 71.9$ km/s/Mpc, $\Omega_b h^2 = 0.02273$, $\Omega_c h^2 = 0.1099$, $n_s = 0.963$ and $\tau = 0.087$. We require $N_{side} = 512$ and a maximum multipole equal to 600.

In the same way, we generate 250 noise maps with noise properties consistent with WMAP Q, W and V frequency bands :

$$N(\hat{\Omega}) = \frac{\sigma_0}{\sqrt{N_{obs}}} n(\hat{\Omega}) \quad (13)$$

where $N(\hat{\Omega})$ is the final noise map obtained from a white noise map $n(\hat{\Omega})$ combined with the WMAP rms noise per observation, σ_0 , and the number of observations per pixel, N_{obs} . We extract N_{obs} from the WMAP 5-year Stokes-I sky maps fits files and take $\sigma_0 = 2.197, 3.133, 6.538$ mK for the Q, V and W 5-year data, respectively, as published on the lambda website by the WMAP team.

We analyze both raw maps as well as foreground-cleaned maps provided by the WMAP team. We show and tabulate results separately for these two options.

We use the Healpix anafast code [27] and the $KQ75$ mask to extract the multipole coefficients for each frequency band out to $l_{max} = 600$ for WMAP maps,

a_{lm}^D , simulated Gaussian maps, a_{lm}^G , and simulated noise maps, a_{lm}^N . The noise spectrum needed for computing the denominators in (8) is obtained averaging the simulated noise spectra over the solid angle and considering the sky-cut according to the relation :

$$N_l = \Omega \int \frac{d^2 \hat{n} \sigma_0^2 M(\hat{n})}{4\pi f_{sky} N_{obs}(\hat{n})}, \quad (14)$$

where $\Omega \equiv 4\pi/N_{pixel}$ is the solid angle per pixel, $M(\hat{n})$ is the $KQ75$ mask and $f_{sky} = 0.718$ is the corresponding observed sky fraction.

We calculate the lensed and unlensed CMB power spectrum with the public CAMB code [35] using again the cosmological parameters from the WMAP 5-year best fit model.

We put everything together to obtain all coefficients in (8) and the relative sky maps considering $a_{lm} = a_{lm}^D$ for data instead, in the case of simulations, we need to consider noise and beam contribution to multipoles: $a_{lm} = a_{lm}^G b_l + a_{lm}^N$, so our gaussian multipoles are convolved with the frequency-dependent beam transfer function b_l and added to the noise multipoles.

B. Skewness power spectrum

We estimate the $C_l^{2,1}$ according to equation (11) for each frequency band and for different lensing-secondary anisotropy cross-correlation power spectrum; in particular, X_l ISW is the spectrum of cross-correlating lensing with Integrate Sachs-Wolfe effect [28] and, in the same way, X_l SZ for Sunyaev-Zel'dovich effect [29] (see Figure 1). We calculate these in the fiducial cosmological model consistent with WMAP 5-year data and making use of the halo model approach to describe the SZ signal [30, 31, 32]. The ISW effect is described through the standard linear power spectrum of the potential field and the CMB lensing potential is also modeled using the linear fluctuations [33, 34].

In Figures 2 and 3 we show all terms of equation (11). It's evident that linear terms are not significant compared to the others coming from data only. However, we are using all the contributions when calculating the skewness spectrum.

In Figure 4 we report both raw and foregrounds-cleaned maps data with all corrective terms considered compared to $C_l^{2,1}$ from Gaussian simulations.

C. Best Fit Parameter Estimation

1. Secondary non-Gaussianity only

At this stage, we make an assumption, relaxed later, that there is no primordial non-Gaussianity.

In Figures 5 and 6 we plot binned data for each X_l configuration and for each frequency band with a $\Delta l = 50$.

¹ <http://lambda.gsfc/nasa.gov>

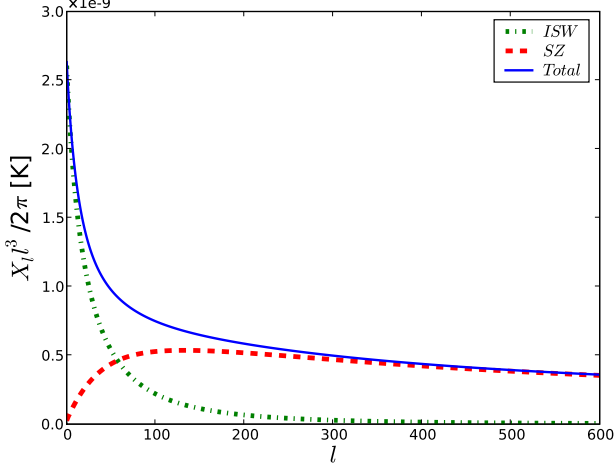


FIG. 1: The lensing-secondary anisotropy cross-correlation power spectrum. We consider two secondary effects here with ISW and SZ as these are the two dominant lensing-secondary correlations expected. The blue solid line is the total contribution when we consider both ISW and SZ effects.

The corresponding error bars are from simulations variance and the solid blue line represents a calculation from the halo model for the lensing-SZ and lensing-ISW correlations. These calculations are described in Ref. [25].

In making these estimates, we also allow for unresolved point sources. We calculated the overlap between the lensing-SZ and lensing-ISW estimators with the point sources given by their shot-noise term of the angular bispectrum. We parameterize point source amplitude such that :

$$B_{l_1 l_2 l_3}^{\text{PS}} = b_{\text{src}} \sqrt{\frac{(2l_1 + 1)(2l_2 + 1)}{4\pi(2l + 1)}} \begin{pmatrix} l_1 & l_2 & l_3 \\ 0 & 0 & 0 \end{pmatrix}, \quad (15)$$

and we consider $b_{\text{src}} = B_i \times 10^{-25} \text{ sr}^2$ as a function of frequency i .

In order to estimate the relative amplitudes of SZ and ISW correlation with the lensing potential as well as the contaminant contribution from unresolved point sources, we compare the data to a model calculation that contains lensing bispectra and the overlap between lensing and point source bispectra :

$$\mathbf{D} = A \times C_l^{2,1 \text{sec-lens}} + B_i \times E_l^{2,1 \text{PS}}, \quad (16)$$

where :

$$E_l^{2,1} = \frac{1}{2l + 1} \sum_{l_1 l_2} \frac{\hat{B}_{l_1 l_2}^{\text{PS}} (B_{l_1 l_2}^{\text{PLS}})^c}{\tilde{C}_l \tilde{C}_{l_1} \tilde{C}_{l_2}}, \quad (17)$$

and $\hat{B}_{l_1 l_2}^{\text{PS}}$ is the point source shot-noise bispectrum described in equation (15). The parameter A denotes the

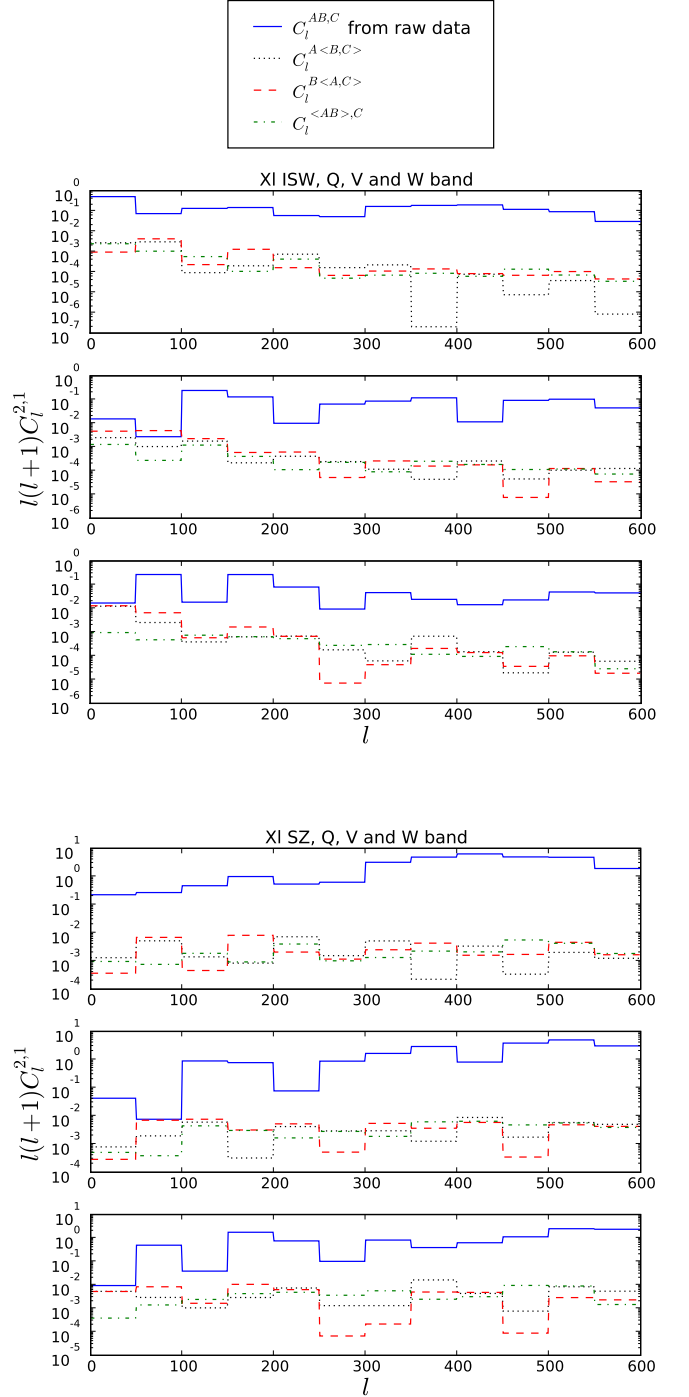


FIG. 2: Corrective terms compared with the raw data estimator for Q, V, and W band for X_l with ISW (top) and SZ (bottom), respectively.

total amplitude of the combined lensing-SZ and lensing-ISW correlations.

In doing the above model fit to multi-frequency measurements of the 2,1 correlator optimized for lensing-secondary correlations, we assume that the lensing-

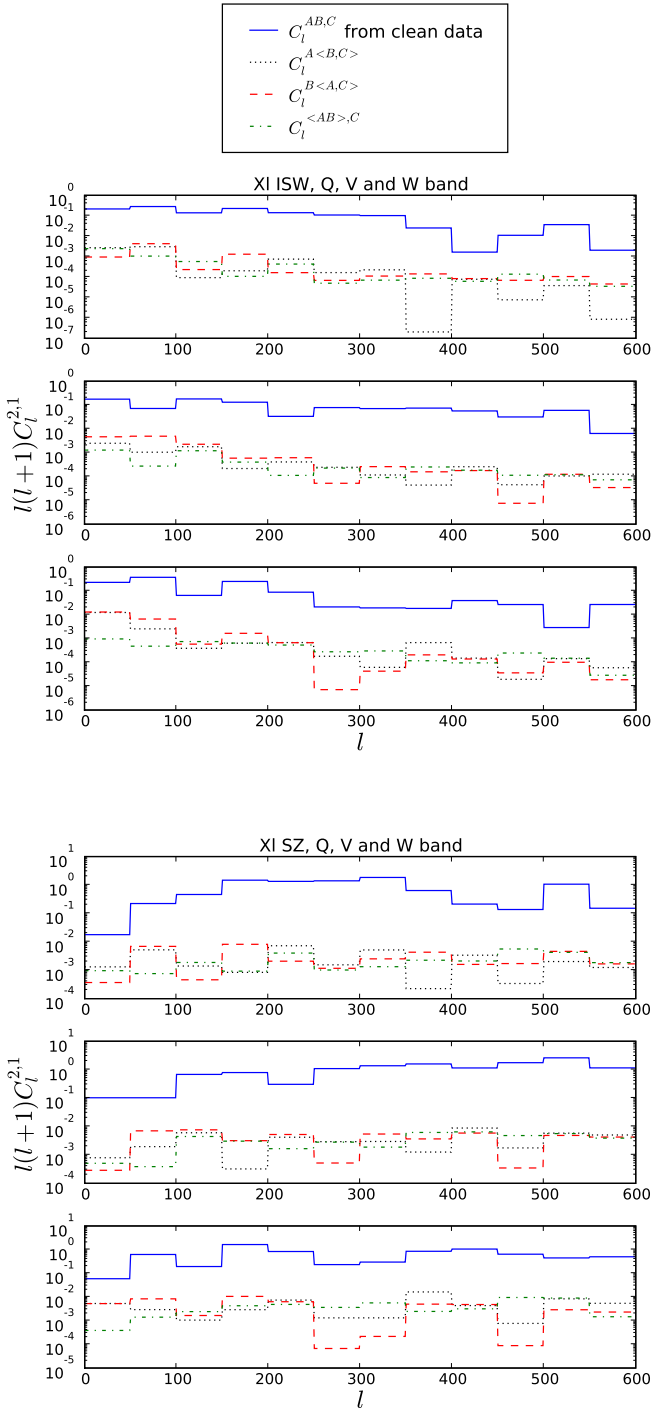


FIG. 3: Corrective terms compared with the clean data estimator for Q, V, and W band for X_l with ISW (top) and with SZ (bottom), respectively.

secondary cross-correlation amplitude is frequency-independent, except for the known frequency dependence of the SZ effect taken as part of the model calculation of X_l . We assume three different amplitudes for point sources in each of Q, V, and W bands of WMAP.

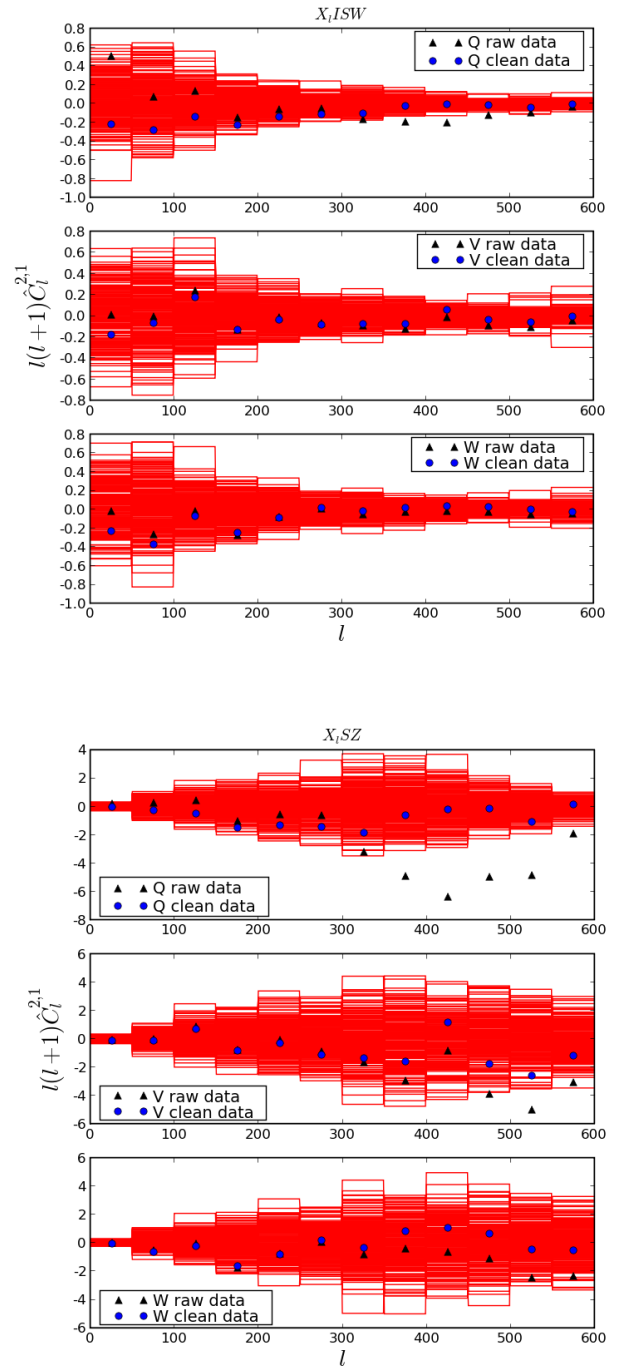


FIG. 4: Binned data obtained calculating all the corrective terms compared to the skew spectrum of simulations for X_l ISW (top) and X_l SZ (bottom).

Our technique as implemented currently does not allow us to separate the lensing-SZ correlation amplitude from lensing-ISW amplitude as the two are found to be highly degenerate with each other. In future, especially with Planck, one may be able to separate lensing-SZ from

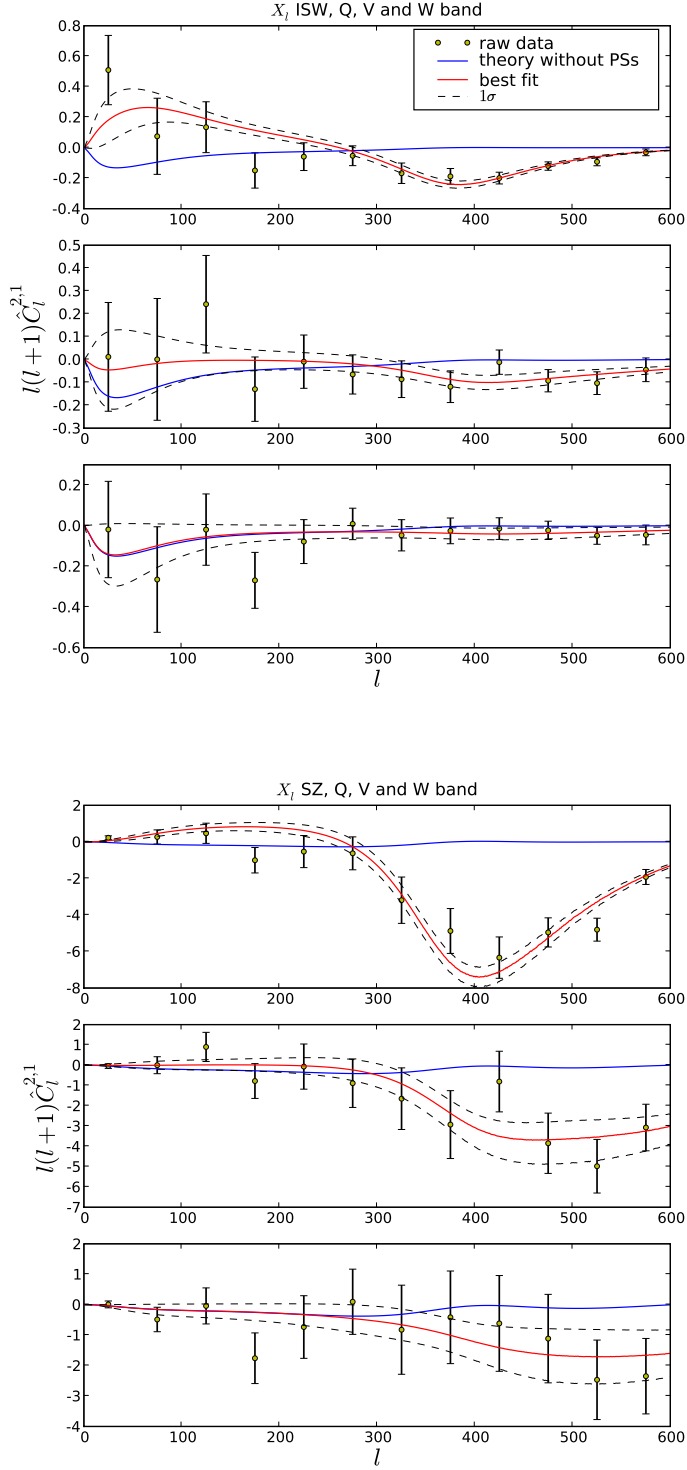


FIG. 5: Q, V and W band WMAP raw data with error bars from simulations variance compared with the theoretical models and the best fit results for X_l ISW (top) and X_l SZ (bottom).

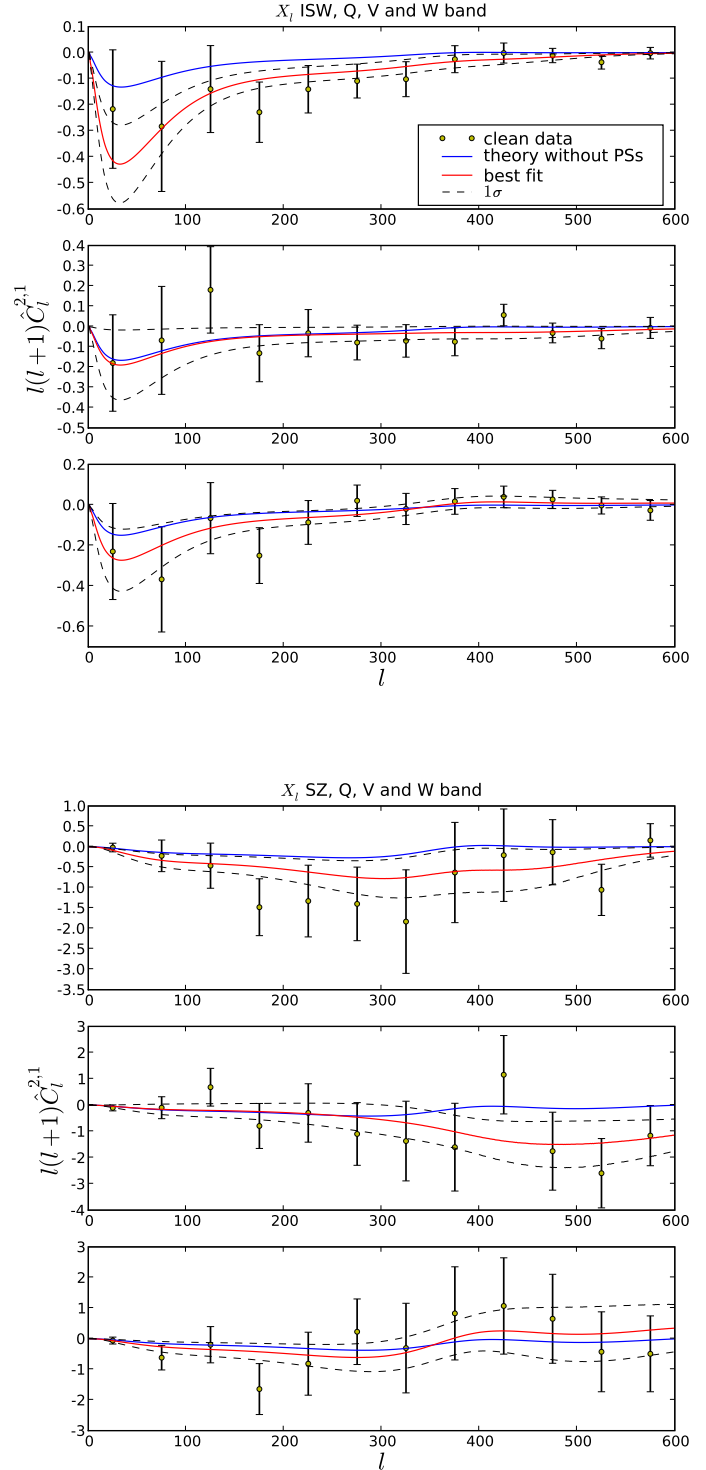


FIG. 6: Q, V and W band WMAP clean data with error bars from simulations variance compared with the theoretical models and the best fit results for X_l ISW (top) and X_l SZ (bottom).

lensing-ISW based on the SZ frequency dependence.

To estimate the amplitudes A and B_i we define a χ^2 merit function :

$$\chi^2 = (\mathbf{y}^T - \mathbf{T} \cdot \mathbf{P})^T \mathbf{C}^{-1} (\mathbf{y} - \mathbf{T} \cdot \mathbf{P}) \quad (18)$$

where \mathbf{y} is the data vector (binned $C_l^{2,1}$ for each frequency band and X_l configuration), \mathbf{T} is the theory matrix and $\mathbf{P} = (A, B_i)$ is the parameter vector that we want to estimate. \mathbf{C} is the covariance matrix from simulations.

To determine the parameters, we minimize the χ^2 function explicitly and obtain the best-fit parameters as :

$$\mathbf{P} = (\mathbf{T}^T \mathbf{C}^{-1} \mathbf{T})^{-1} (\mathbf{T}^T \mathbf{C}^{-1} \mathbf{y}) \quad (19)$$

and the error bars are obtained by the diagonal elements of the following matrix :

$$\sigma_{\mathbf{P}}^2 = (\mathbf{T}^T \mathbf{C}^{-1} \mathbf{T})^{-1} . \quad (20)$$

We summarize results related to the amplitude determination for different frequency bands in the tables I and II for raw and foreground-cleaned maps respectively. We categorize our results by the choice we make in setting X_l while generating C maps. Here, X_l forms a template to search for the lensing-secondary cross-correlation. In $C_l^{2,1}$, due to weighting, one of the bispectra probes the total non-Gaussianity in CMB data that could come from a combination of effects from primordial non-Gaussianity to lensing and radio point sources. The second bispectrum forces a certain configuration and the overlap between the total and the assumed shape of the bispectrum determines the shape of $C_l^{2,1}$ measured from the data. By setting a function for X_l , we set the overall normalization of the prescribed lensing-secondary cross-correlation bispectrum. Thus the amplitude A we determine from the data is simply the overall amplitude of the non-Gaussianity associated with the overlap between lensing-secondary cross-correlation and all forms of non-Gaussianities that are present in the data. We remove the confusion associated with point sources, which is expected to be significant, by explicitly calculating the overlap between lensing-(SZ+ISW) bispectrum and the shot-noise form of the point source bispectrum.

After accounting for the confusion from point sources generated by the overlap of the point source shot-noise bispectrum and the lensing-secondary anisotropy cross-correlation bispectrum, we find no significant detection of the lensing effect in existing WMAP data. We constrain the overall normalization of the lensing-SZ and lensing-ISW angular cross-power spectra to be 0.42 ± 0.86 and 1.19 ± 0.86 in combined V and W-band raw and foreground-cleaned maps provided by the WMAP team, respectively. The point source amplitude we determine from the raw map of Q-band with $b_{\text{src}} = (67.8 \pm 5.4) \times 10^{-25} \text{ sr}^2$ is higher than the estimate by the WMAP team with $(6.0 \pm 1.3) \times 10^{-5} \mu\text{K}^3\text{-sr}^2$ [2] (the value we determine is $(13.7 \pm 1.1) \times 10^{-5} \mu\text{K}^3\text{-sr}^2$ in the same units used by the WMAP team). We find similarly a factor of 2 increase in V-band map as well.

In the case of clean maps, we find $b_{\text{src}} = (6.2 \pm 5.4) \times 10^{-25} \text{ sr}^2$, which is smaller than the WMAP team's estimate with clean maps for the Q band with $(4.3 \pm 1.3) \times 10^{-5} \mu\text{K}^3\text{-sr}^2$ [2] (the value we determine is $(1.4 \pm 1.1) \times 10^{-5} \mu\text{K}^3\text{-sr}^2$ in the same units used by the WMAP team). We find similar differences in V and W-band as well.

It is unclear exactly where these differences come from. We do not employ the same E-statistic that is optimized for point sources as the WMAP team in the present study.

2. Inclusion of primordial non-Gaussianity

To study the impact of primordial non-Gaussianity we now fit the data by modifying equation (16) to include a local form of non-Gaussianity with amplitude f_{NL} :

$$\mathbf{D} = A \times C_l^{2,1\text{sec-lens}} + B_i \times E_l^{2,1\text{PS}} + f_{\text{NL}} Y_l^{2,1\text{prim}} , \quad (21)$$

where now :

$$Y_l^{2,1} = \frac{1}{2l+1} \sum_{l_1 l_2} \frac{\hat{B}_{ll_1 l_2}^{\text{prim}} (B_{ll_1 l_2}^{\text{PLS}})^c}{\tilde{C}_l \tilde{C}_{l_1} \tilde{C}_{l_2}} , \quad (22)$$

involves the overlap between lensing-secondary and primordial non-Gaussianities with the overall amplitude of the primordial non-Gaussianity determined by f_{NL} [9, 12].

Including primordial non-Gaussianity confuses the detection of lensing-secondary correlations and leads to a factor of 2 degradation in the error of the amplitude of lensing-secondary correlation power spectrum (see Table III). The estimator as constituted is not optimised to detect primordial non-Gaussianity, and we find a rather weaker limit of $f_{\text{NL}} = -13 \pm 62$ from the clean V+W maps, with a larger error bar than in the study of Ref. [9] which uses the optimised estimator of Ref. [24] for primordial non-Gaussianity specifically.

We emphasize that our current study is more focused towards a detection of the lensing-secondary correlation in WMAP data. In an upcoming paper, we will present a combined analysis of three estimators of the 2,1 correlator optimized separately for primordial non-Gaussianity, point sources, and lensing effects.

In Figure 7 we report the two dimensional countour plots showing degeneracies between our best fit parameters for raw and clean maps from the WMAP team used for the data analysis.

IV. CONCLUSIONS

We measure the skewness power spectrum of the CMB anisotropies optimized for a detection of the secondary bispectrum generated by the correlation of the CMB lensing potential with integrated Sachs-Wolfe effect and the

Frequency	X_l	A	B_Q	B_V	B_W	χ^2/dof
Q	SZ+ISW	-1.59 ± 1.21	67.8 ± 5.4	11.4 ± 2.4		1.67
V		0.06 ± 1.08				0.85
W		1.01 ± 1.06	67.8 ± 5.2	12.4 ± 2.2	5.4 ± 2.6	0.58
Q+W+V		0.07 ± 0.82			5.8 ± 2.4	1.22
W+V		0.42 ± 0.86			5.2 ± 2.6	0.82
Q	ISW	-1.03 ± 1.19	123.4 ± 12.4	20.8 ± 6.2		1.02
V		0.33 ± 1.06				0.67
W		0.99 ± 1.05	128.2 ± 11.8	22.6 ± 5.8	10.0 ± 7.0	0.50
Q+W+V		0.43 ± 0.82			11.6 ± 6.6	1.02
W+V		0.48 ± 0.86			8.4 ± 6.8	0.66
Q	SZ	-1.47 ± 1.33	136.0 ± 10.8	22.8 ± 4.6		1.68
V		0.24 ± 1.18				0.84
W		1.09 ± 1.14	136.2 ± 10.4	25.2 ± 4.2	10.8 ± 5.2	0.60
Q+W+V		0.13 ± 0.89			12.2 ± 5.0	1.23
W+V		0.57 ± 0.94			10.4 ± 5.0	0.85

TABLE I: Amplitude parameters estimation using WMAP raw maps.

Frequency	X_l	A	B_Q	B_V	B_W	χ^2/dof
Q	SZ+ISW	2.93 ± 1.21	6.2 ± 5.4			0.55
V		0.93 ± 1.08				4.4 ± 2.4
W		1.73 ± 1.06	8.8 ± 5.2	4.2 ± 2.2	-1.3 ± 2.6	0.46
Q+W+V		1.56 ± 0.82			-1.4 ± 2.4	0.82
W+V		1.19 ± 0.86			-1.6 ± 2.6	0.77
Q	ISW	3.32 ± 1.19	17.2 ± 12.6	5.8 ± 6.4		0.34
V		1.16 ± 1.06				0.62
W		1.81 ± 1.05	25.4 ± 11.8	5.6 ± 5.8	-4.3 ± 7.0	0.42
Q+W+V		1.76 ± 0.82			-5.4 ± 6.6	0.86
W+V		1.33 ± 0.86			-6.0 ± 6.8	0.67
Q	SZ	2.58 ± 1.33	12.2 ± 10.8	8.7 ± 4.7		0.62
V		0.99 ± 1.18				0.70
W		1.66 ± 1.14	16.6 ± 10.4	8.2 ± 4.4	-2.5 ± 5.2	0.49
Q+W+V		1.47 ± 0.89			-2.2 ± 5.0	0.69
W+V		1.22 ± 0.93			-3.0 ± 5.0	0.80

TABLE II: Amplitude parameters estimation using WMAP foreground cleaned maps.

Sunyaev-Zel'dovich effect. The covariance of our measurements are generated by Monte-Carlo simulations of Gaussian CMB fields with noise properties consistent with WMAP.

When interpreting multi-frequency measurements we also take into account the confusion resulting from the unresolved radio point sources. We analyze Q, V and W-band WMAP 5-year raw and foreground cleaned maps using the KQ75 mask out to $l_{\max} = 600$.

While with the raw maps we find no evidence for a non-zero non-Gaussian signal from the lensing-secondary correlation in any of the three bands, we find 2σ and 3σ

evidence for a non-zero amplitude of both the lensing-ISW and lensing-SZ signals in the foreground cleaned Q-band map provided by the WMAP team, respectively. The point source amplitude at the bispectrum level measured with this skewness power spectrum is consistent with previous measurements using the optimized skewness of the WMAP team's analysis and a different form of the skewness power spectrum optimized for point sources.

Finally, as the focus is on secondary non-Gaussianity, the estimator is not optimised to detect primordial non-Gaussian signals, and we find a limit on local type of $f_{\text{NL}} = -13 \pm 62$ from cleaned V+W maps.

Frequency	Data	A	B_Q	B_V	B_W	f_{NL}	χ^2/dof			
Q	Raw	0.39 ± 1.99	69.8 ± 5.6	11.3 ± 2.4	5.6 ± 2.6	-95 ± 76	1.68			
V		-0.51 ± 1.78				31 ± 70	0.92			
W		2.18 ± 1.78				-60 ± 73	0.56			
Q+W+V		1.58 ± 1.46				68.6 ± 5.2	12.2 ± 2.1	5.8 ± 2.5	-70 ± 56	0.60
W+V		0.75 ± 1.56				11.9 ± 2.2	5.1 ± 2.5	-16 ± 62	0.85	
Q	Clean	2.02 ± 1.99	5.3 ± 5.6	4.2 ± 2.4	-1.1 ± 2.6	43 ± 76	0.58			
V		-0.03 ± 1.78				48 ± 70	0.73			
W		3.04 ± 1.78				-67 ± 73	0.42			
Q+W+V		1.59 ± 1.46				8.9 ± 5.2	4.1 ± 2.2	-1.4 ± 2.5	0 ± 56	0.39
W+V		1.47 ± 1.56				4.9 ± 2.3	-1.6 ± 2.5	-13 ± 62	0.80	

TABLE III: Amplitude parameters estimation using WMAP raw and clean maps for X_l total and including an extra parameter related to primordial non-Gaussianity.

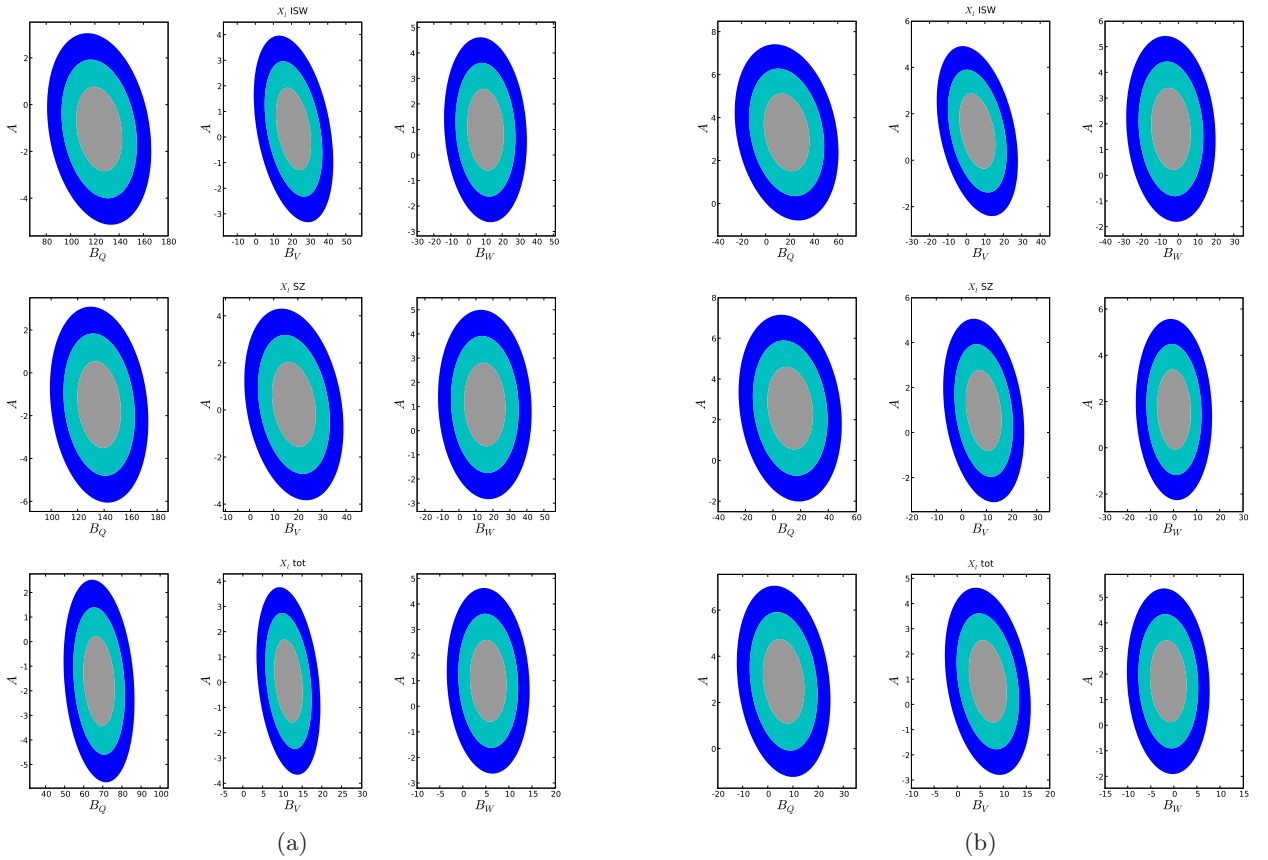


FIG. 7: 2-dimensional contour plots showing the degeneracies at 68%, 95% and 99.7% confidence levels between the best fit parameters from raw (left panel (a)) and clean (right panel (b)) map data analysis for the ISW (top), SZ (middle) and joint ISW+SZ (bottom) cases.

- [1] G. Hinshaw *et al.* [WMAP Collaboration], arXiv:0803.0732 [astro-ph];
 [2] E. Komatsu *et al.*, arXiv:0803.0547 [astro-ph].
 [3] J. Dunkley *et al.* [WMAP Collaboration], *Astrophys. J.*

- Suppl. **180**, 306 (2009) [arXiv:0803.0586 [astro-ph]].
 [4] C. Copi, D. Huterer, D. Schwarz and G. Starkman, *Phys. Rev. D* **75**, 023507 (2007) [arXiv:astro-ph/0605135].
 [5] J. Hoftuft, H. K. Eriksen, A. J. Banday, K. M. Gorski,

- F. K. Hansen and P. B. Lilje, *Astrophys. J.* **699**, 985 (2009) [arXiv:0903.1229 [astro-ph.CO]].
- [6] D. Hanson and A. Lewis, arXiv:0908.0963 [astro-ph.CO].
- [7] J. P. Luminet, J. Weeks, A. Riazuelo, R. Lehoucq and J. P. Uzan, *Nature* **425**, 593 (2003) [arXiv:astro-ph/0310253].
- [8] B. F. Roukema, B. Lew, M. Cechowska, A. Marecki and S. Bajtlik, *Astron. Astrophys.* **423**, 821 (2004) [arXiv:astro-ph/0402608].
- [9] J. Smidt, A. Amblard, P. Serra and A. Cooray, arXiv:0907.4051 [astro-ph.CO].
- [10] L. Senatore, K. M. Smith and M. Zaldarriaga, arXiv:0905.3746 [astro-ph.CO].
- [11] D. Pietrobon, P. Cabella, A. Balbi, G. de Gasperis and N. Vittorio, arXiv:0812.2478 [astro-ph].
- [12] K. M. Smith, L. Senatore and M. Zaldarriaga, arXiv:0901.2572 [astro-ph].
- [13] J. M. Maldacena, *JHEP* **0305**, 013 (2003) [arXiv:astro-ph/0210603].
- [14] M. Sasaki and E. D. Stewart, *Prog. Theor. Phys.* **95**, 71 (1996) [arXiv:astro-ph/9507001].
- [15] D. H. Lyth, K. A. Malik and M. Sasaki, *JCAP* **0505**, 004 (2005) [arXiv:astro-ph/0411220].
- [16] D. H. Lyth and Y. Rodriguez, *Phys. Rev. Lett.* **95**, 121302 (2005) [arXiv:astro-ph/0504045].
- [17] V. Acquaviva, N. Bartolo, S. Matarrese and A. Riotto, *Nucl. Phys. B* **667**, 119 (2003) [arXiv:astro-ph/0209156].
- [18] A. Cooray, *Phys. Rev. D* **64**, 063514 (2001) [arXiv:astro-ph/0105063].
- [19] L. Verde and D. N. Spergel, *Phys. Rev. D* **65**, 043007 (2002) [arXiv:astro-ph/0108179].
- [20] D. M. Goldberg and D. N. Spergel, *Phys. Rev. D* **59**, 103002 (1999) [arXiv:astro-ph/9811251].
- [21] A. R. Cooray and W. Hu, *Astrophys. J.* **534**, 533 (2000) [arXiv:astro-ph/9910397].
- [22] A. P. S. Yadav and B. D. Wandelt, *Phys. Rev. Lett.* **100**, 181301 (2008) [arXiv:0712.1148 [astro-ph]].
- [23] A. Cooray, *Phys. Rev. D* **64**, 043516 (2001) [arXiv:astro-ph/0105415].
- [24] D. Munshi and A. Heavens, arXiv:0904.4478 [astro-ph.CO].
- [25] D. Munshi, P. Valageas, A. Cooray and A. Heavens, arXiv:0907.3229 [astro-ph.CO].
- [26] K. M. Smith and M. Zaldarriaga, arXiv:astro-ph/0612571.
- [27] K. M. Gorski, E. Hivon, A. J. Banday, B. D. Wandelt, F. K. Hansen, M. Reinecke and M. Bartelman, *Astrophys. J.* **622**, 759 (2005) [arXiv:astro-ph/0409513].
- [28] R. K. Sachs and A. M. Wolfe, *Astrophys. J.* **147**, 73 (1967) [*Gen. Rel. Grav.* **39**, 1929 (2007)].
- [29] R. A. Sunyaev and Y. B. Zeldovich, *Ann. Rev. Astron. Astrophys.* **18**, 537 (1980).
- [30] A. Cooray and R. K. Sheth, *Phys. Rept.* **372**, 1 (2002) [arXiv:astro-ph/0206508].
- [31] A. Cooray, *Phys. Rev. D* **62**, 103506 (2000) [arXiv:astro-ph/0005287].
- [32] E. Komatsu and U. Seljak, *Mon. Not. Roy. Astron. Soc.* **336**, 1256 (2002) [arXiv:astro-ph/0205468].
- [33] N. Afshordi, *Phys. Rev. D* **70**, 083536 (2004) [arXiv:astro-ph/0401166].
- [34] A. Cooray, *Phys. Rev. D* **65**, 103510 (2002) [arXiv:astro-ph/0112408].
- [35] A. Lewis, A. Challinor and A. Lasenby, *Astrophys. J.* **538** (2000) 473 [arXiv:astro-ph/9911177].